SAND2020-8091C

Matrix Completion for Compressive Sensing Using Consensus Equilibrium

Dennis J. Lee

Sandia National Laboratories, 1515 Eubank Blvd., Albuquerque, NM 87123

ABSTRACT

We propose a technique for reconstruction from incomplete compressive measurements. Our approach combines compressive sensing and matrix completion using the consensus equilibrium framework. Consensus equilibrium breaks the reconstruction problem into subproblems to solve for the high-dimensional tensor. This framework allows us to apply two constraints on the statistical inversion problem. First, matrix completion enforces a low rank constraint on the compressed data. Second, the compressed tensor should be consistent with the uncompressed tensor when it is projected onto the low-dimensional subspace. We validate our method on the Indian Pines hyperspectral dataset with varying amounts of missing data. This work opens up new possibilities for data reduction, compression, and reconstruction.

Keywords: Matrix completion, compressive sensing, consensus equilibrium, hyperspectral imaging

1. INTRODUCTION

Cameras are now able to capture data exceeding $>$ 1 gigapixel, $>$ 10,000 frames per second, and $>$ 100 color channels. Data rates can potentially reach 1×10^{15} pixels per second. Such high data rates make real-time processing difficult.

Efficient sensing takes advantage of low-dimensional structure in signals. Two areas of research explore prior structured knowledge: compressive sensing and matrix completion. Compressive sensing permits few linear measurements of a signal with nearly exact reconstruction. Matrix completion aims to estimate incomplete observations living in a low rank subspace.

We propose to recover an uncompressed tensor from incomplete compressive measurements by combining these techniques. Consensus equilibrium breaks the reconstruction problem into subproblems to solve for the high-dimensional tensor. This framework allows us to apply two constraints on the statistical inversion problem. First, matrix completion enforces a low rank constraint on the compressed data. Second, the compressed tensor should be consistent with the uncompressed tensor when it is projected into the lower dimensional space. We validate our method on the Indian Pines hyperspectral dataset with varying amounts of missing data. This work opens up new possibilities for data reduction, compression, and reconstruction. This section introduces some key concepts used in this paper.

Compressive sensing exploits the inherent structure and redundancy within an acquired signal. Image and video compression algorithms operating on commercial 10 megapixel cameras can achieve compression ratios of 100:1 or higher for visualization or classification tasks, illustrating the redundancy in natural images.

Suppose a vector has N components, and $S < N$ components are non-zero. We wish to take M measurements using a random sensing strategy. Compressive sensing theory says that if M is approximately greater than $S \log N$, we can recover the N components with high probability.[1] The signal may be S-sparse under a transform, such as the Discrete Cosine Transform or wavelet transform.[2] Applications include digital holography,[3] video coding,[4] optical polarimetry,[5,6] image processing,[7] and communications.

A key notion in compressive sensing is the restricted isometry property (RIP).[8] If a matrix $\boldsymbol{A}$ satisfies the RIP, then $\boldsymbol{A}$ approximately preserves the Euclidean length of S-sparse signals. This implies that all pairwise

Further author information: (Send correspondence to D.J.L.)
D.J.L.: E-mail: dlee1@sandia.gov

Sandia National Laboratories is a multimission laboratory managed and operated by National Technology & Engineering Solutions of Sandia, LLC, a wholly owned subsidiary of Honeywell International Inc., for the U.S. Department of Energy's National Nuclear Security Administration under contract DE-NA0003525.

distances between S-sparse signals must be well preserved in measurement space. In other words, the distance between two low-dimensional subspaces remain almost unchanged after projection by a random matrix with overwhelming probability. We hypothesize that low-rank matrices remain low-rank after projection. Under this hypothesis, we can perform matrix completion on the compressive measurements.

Matrix completion finds applications in signal processing, computer vision, and control theory. It aims to generate a completed matrix from missing entries. Observed entries may be corrupted by erasures and transmission errors, scene occlusions, deliberate omissions, or bad pixels.[9] Candes and Tao provide a theoretical guarantee for exact matrix retrieval under nuclear norm convex relaxation.[10] Other formulations factor a matrix $\boldsymbol{A} = \boldsymbol{U}\boldsymbol{V}$ with gradient updates for $\boldsymbol{U}$ and $\boldsymbol{V}$.[11] In this work, we are not directly interested in recovering the missing entries from the compressive measurements. Rather, the end goal is to reconstruct the uncompressed tensor from incomplete compressive measurements.

Statistical inversion techniques minimize an objective involving data fidelity and regularization terms using the maximum a posteriori estimate.[12] Efficient minimization methods such as alternating direction method of multipliers (ADMM) can apply different proximal maps in sequence.[13,14] However, many inverse problems cannot be framed in terms of a explicit objective.[15–18] Consensus equilibrium is an optimization-free generalization of regularized inversion that can fuse multiple sources of information.[19] Applications include tomography and denoising.[20] Here we demonstrate a novel problem of reconstruction from incomplete compressive measurements.

2. THEORY

2.1 Notation

Throughout this paper, we follow standard tensor notation from Kolda.[21] Let $\boldsymbol{\mathcal{X}} \in \mathbb{R}^{M \times N \times B}$ denote a three-way tensor with dimensions $M \times N \times B$. The mode-3 unfolding of this tensor is

$$\boldsymbol{X} \coloneqq \boldsymbol{X}_{(3)} \in \mathbb{R}^{B \times (M \times N)}. \tag{1}$$

Let $\boldsymbol{A} \in \mathbb{R}^{R \times B}$ denote a matrix that encodes the measurement of $\boldsymbol{\mathcal{X}}$. Here B represents the signal length, while R is the number of measurements, with $R < B$. Denote $\boldsymbol{\mathcal{Y}} \in \mathbb{R}^{M \times N \times R}$ as the tensor of measurements. It is a compressed version of $\boldsymbol{\mathcal{X}}$:

$$\boldsymbol{\mathcal{Y}} = \boldsymbol{\mathcal{X}} \times_3 \boldsymbol{A} \tag{2}$$

where $\times_3$ is a tensor 3-mode product. Define $\boldsymbol{Y}$ as the mode-3 unfolding of this tensor:

$$\boldsymbol{Y} \coloneqq \boldsymbol{Y}_{(3)} \in \mathbb{R}^{R \times (M \times N)}. \tag{3}$$

Here the third dimension of $\boldsymbol{\mathcal{X}}$ is compressed from size B to size R. The compression ratio is

$$\kappa = \frac{R}{B}. \tag{4}$$

We index the complete set of measurements as

$$\Omega = \{1, 2, \ldots, M \times N \times R\}. \tag{5}$$

Define ω as the set of observations, which may not include all of the possible measurements:

$$\omega \subset \Omega = \{1, 2, \ldots, M \times N \times R\}. \tag{6}$$

If entry (i, j, k) is unobserved, we use the shorthand that $(i, j, k) \notin \omega$. The fraction of missing entries is

$$\mu = 1 - \frac{|\omega|}{M \times N \times R}. \tag{7}$$

Notice that the original tensor $\boldsymbol{\mathcal{X}}$ is reduced in the number of entries through two steps:

1. Compression by $\boldsymbol{A}$ to yield $\boldsymbol{\mathcal{Y}}$, and
2. Projection onto a set of observations to yield $\mathcal{P}_\omega(\boldsymbol{\mathcal{Y}}) \in \mathbb{R}^{M \times N \times R}$, where the sampling operator $\mathcal{P}_\omega(\cdot)$ returns the original tensor but with the (i, j, k) entry denoted as missing if $(i, j, k) \notin \omega$.

After these steps, the total number of measurements τ becomes

$$\tau = \kappa(1 - \mu). \tag{8}$$

2.2 Compressive sensing

The goal is to recover $\boldsymbol{\mathcal{X}}$ from $\mathcal{P}_\omega(\boldsymbol{\mathcal{Y}})$. We consider the subproblems of reconstructing the mode-3 fibers $\boldsymbol{x}_i \in \mathbb{R}^B$ for $i = 1, 2, \ldots, M \times N$. Let $\boldsymbol{W} \in \mathbb{R}^{B \times B}$ denote the inverse of a transform which represents a signal in terms of sparse coefficients. It may represent wavelet or Fourier transforms, for example. Write the coefficients as $\tilde{\boldsymbol{x}}_i \in \mathbb{R}^B$ for $i = 1, 2, \ldots, M \times N$. The corresponding measurements are the mode-3 fibers of $\boldsymbol{\mathcal{Y}}$: $\boldsymbol{y}_i \in \mathbb{R}^R$ for $i = 1, 2, \ldots, M \times N$. A solution to this problem is provided by basis pursuit with denoising parameter σ:

$$\begin{aligned} \underset{\tilde{\boldsymbol{x}}_i}{\text{minimize}} \quad & ||\tilde{\boldsymbol{x}}_i||_1 \\ \text{subject to} \quad & ||\boldsymbol{A}\boldsymbol{W}\tilde{\boldsymbol{x}}_i - \boldsymbol{y}_i||_2 \leq \sigma. \end{aligned} \tag{9}$$

We adapt the spectral projected gradient algorithm presented by van den Berg and Friedlander.[22] Algorithm 1 formalizes the optimization problem to recover $\boldsymbol{\mathcal{X}}$.

Algorithm 1 Basis pursuit with denoising

procedure BP($\boldsymbol{\mathcal{Y}}$, $\boldsymbol{A}$, $\boldsymbol{W}$, σ)
  for $i = 1, \ldots, M \times N$ **do**
    Solve for $\tilde{\boldsymbol{x}}_i$ according to

$$\begin{aligned} \underset{\tilde{\boldsymbol{x}}_i}{\text{minimize}} \quad & ||\tilde{\boldsymbol{x}}_i||_1 \\ \text{subject to} \quad & ||\boldsymbol{A}\boldsymbol{W}\tilde{\boldsymbol{x}}_i - \boldsymbol{y}_i||_2 \leq \sigma \end{aligned}$$

    $\boldsymbol{x}_i \leftarrow \boldsymbol{W}\ \tilde{\boldsymbol{x}}_i$
  end for
  return $\boldsymbol{\mathcal{X}}$
end procedure

2.3 Matrix completion

The problem of matrix completion is to recover a matrix of rank k with missing entries. This rank k constraint allows a matrix $\boldsymbol{Y} \in \mathbb{R}^{R \times (M \times N)}$ to be factored into two matrices, $\boldsymbol{U} \in \mathbb{R}^{R \times k}$ and $\boldsymbol{S} \in \mathbb{R}^{k \times (M \times N)}$. Here $\boldsymbol{U}$ represents a rank k subspace, and $\boldsymbol{S}$ are the k features for each pixel. We can solve the following optimization problem:

$$\begin{aligned} \underset{||\boldsymbol{S}||_2 = 1}{\text{minimize}} \quad \underset{\boldsymbol{U}}{\text{minimize}} \quad & \frac{1}{R}\left(\sum_{(i,j)\in\Omega}(\widehat{\boldsymbol{Y}}_{ij} - \boldsymbol{Y})^2 + \frac{1}{\gamma}||\boldsymbol{U}||_2^2\right) \\ \text{subject to} \quad & \widehat{\boldsymbol{Y}} = \boldsymbol{U}\boldsymbol{S}. \end{aligned} \tag{10}$$

Various solutions to the matrix completion problem have been proposed. We will utilize the projected gradient descent implementation presented by Bertsimas and Li.[23] Algorithm 2 formalizes the optimization problem to recover $\widehat{\boldsymbol{Y}}$.

The measurements $\mathcal{P}_\omega(\boldsymbol{\mathcal{Y}})$ contain missing entries. We can define the following constraints on the full measurement tensor $\boldsymbol{\mathcal{Y}}$:

1. Consistency constraint using projections. Suppose the uncompressed tensor $\boldsymbol{\mathcal{X}}_0$ is given. Then $\boldsymbol{\mathcal{Y}}$ should satisfy

$$\boldsymbol{\mathcal{Y}}_{\text{proj}} = \boldsymbol{\mathcal{X}}_0 \times_3 \boldsymbol{A}$$

   or equivalently,

$$\boldsymbol{Y}_{\text{proj}} = \boldsymbol{A}\boldsymbol{X}_0. \tag{11}$$

   We set the missing entries as

$$\mathcal{P}_{\Omega\setminus\omega}(\boldsymbol{Y}) = \mathcal{P}_{\Omega\setminus\omega}(\boldsymbol{Y}_{\text{proj}}) \tag{12}$$

Algorithm 2 Matrix completion

procedure MC($\boldsymbol{\mathcal{Y}}$, k, γ, Ω, ω)

Solve for $\hat{\boldsymbol{Y}}$ according to

$$\begin{aligned} \underset{||\boldsymbol{S}||_2=1}{\text{minimize}} \quad & \underset{\boldsymbol{U}}{\text{minimize}} \quad \frac{1}{R}\left(\sum_{(i,j)\in\Omega}(\widehat{\boldsymbol{Y}}_{ij}-\boldsymbol{Y}_{ij})^2+\frac{1}{\gamma}||\boldsymbol{U}||_2^2\right) \\ \text{subject to} \quad & \widehat{\boldsymbol{Y}}=\boldsymbol{U}\boldsymbol{S} \end{aligned}$$

return $\widehat{\boldsymbol{Y}}$

end procedure

Algorithm 3 Consistency constraint using projections

procedure BP-PROJ($\boldsymbol{\mathcal{X}}_0$; $\boldsymbol{Y}$, $\boldsymbol{A}$, $\boldsymbol{W}$, Ω, ω)

$\boldsymbol{Y}_{\text{proj}} \leftarrow \boldsymbol{A}\boldsymbol{X}_0$

$\mathcal{P}_{\Omega\setminus\omega}(\boldsymbol{Y}) \leftarrow \mathcal{P}_{\Omega\setminus\omega}(\boldsymbol{Y}_{\text{proj}})$

$\boldsymbol{\mathcal{X}} \leftarrow \text{BP}(\boldsymbol{\mathcal{Y}}, \boldsymbol{A}, \boldsymbol{W}, \sigma)$

return $\boldsymbol{\mathcal{X}}$

end procedure

where $\Omega\setminus\omega$ is the set of missing entries. Basis pursuit provides an estimate $\boldsymbol{\mathcal{X}}$ from the projected measurement tensor. The two tensors $\boldsymbol{\mathcal{X}}$ and $\boldsymbol{\mathcal{X}}_0$ should be consistent. Algorithm 3 describes an implementation of this consistency constraint using projections.

2. Low rank constraint using matrix completion. We impose a constraint on the measurement tensor $\boldsymbol{\mathcal{Y}}$ to be low rank. The matrix completion algorithm produces $\boldsymbol{Y}_{\text{MC}}$. We set the missing entries as

$$\mathcal{P}_{\Omega\setminus\omega}(\boldsymbol{Y}) = \mathcal{P}_{\Omega\setminus\omega}(\boldsymbol{Y}_{\text{MC}}). \tag{13}$$

Basis pursuit produces the uncompressed tensor $\boldsymbol{\mathcal{X}}$ from the matrix completion estimate. Algorithm 4 implements this low rank constraint based on matrix completion. The procedure BP-MC takes $\boldsymbol{X}_0$ as a dummy argument. It will become a mathematical convenience for later use.

Algorithm 4 Low rank constraint using matrix completion

procedure BP-MC($\boldsymbol{\mathcal{X}}_0$; $\boldsymbol{Y}$, $\boldsymbol{A}$, $\boldsymbol{W}$, ω, Ω)

$\boldsymbol{Y}_{\text{MC}} \leftarrow \text{MC}(\boldsymbol{\mathcal{Y}}, k, \gamma, \omega, \Omega)$

$\mathcal{P}_{\Omega\setminus\omega}(\boldsymbol{Y}) \leftarrow \mathcal{P}_{\Omega\setminus\omega}(\boldsymbol{Y}_{\text{MC}})$

$\boldsymbol{\mathcal{X}} \leftarrow \text{BP}(\boldsymbol{\mathcal{Y}}, \boldsymbol{A}, \boldsymbol{W}, \sigma)$

return $\boldsymbol{\mathcal{X}}$

end procedure

2.4 Consensus equilibrium

Consensus equilibrium is a framework to break a reconstruction problem into subproblems that can be solved separately. We define the tensor valued maps, $F_1, F_2 : \mathbb{R}^{M\times N\times B} \to \mathbb{R}^{M\times N\times B}$:

$$F_1(\boldsymbol{\mathcal{V}}_1) \coloneqq \text{BP-proj}(\boldsymbol{\mathcal{V}}_1; \boldsymbol{Y}, \boldsymbol{A}, \boldsymbol{W}, \Omega, \omega) \tag{14}$$

and

$$F_2(\boldsymbol{\mathcal{V}}_2) \coloneqq \text{BP-MC}(\boldsymbol{\mathcal{V}}_2; \boldsymbol{Y}, \boldsymbol{A}, \boldsymbol{W}, k, \gamma, \Omega, \omega) \tag{15}$$

where $\boldsymbol{\mathcal{V}}_1, \boldsymbol{\mathcal{V}}_2 \in \mathbb{R}^{M\times N\times B}$ and $\boldsymbol{Y}, \boldsymbol{A}, \boldsymbol{W}, k, \gamma, \Omega, \omega$ are given. Further, let us concatenate the tensors and maps using the following notation:

$$\boldsymbol{\mathcal{V}} = \begin{bmatrix} \boldsymbol{\mathcal{V}}_1 \\ \boldsymbol{\mathcal{V}}_2 \end{bmatrix} \in \mathbb{R}^{M\times N\times B\times 2} \tag{16}$$

and

$$\boldsymbol{F}(\boldsymbol{\mathcal{V}}) = \begin{bmatrix} F_1(\boldsymbol{\mathcal{V}}_1) \\ F_2(\boldsymbol{\mathcal{V}}_2) \end{bmatrix} \in \mathbb{R}^{M\times N\times B\times 2}. \tag{17}$$

Define another tensor valued map $\boldsymbol{G} : \mathbb{R}^{M\times N\times B\times 2} \to \mathbb{R}^{M\times N\times B\times 2}$ as

$$\boldsymbol{G}(\boldsymbol{\mathcal{V}}) = \begin{bmatrix} \overline{\boldsymbol{\mathcal{V}}} \\ \overline{\boldsymbol{\mathcal{V}}} \end{bmatrix} \tag{18}$$

Here

$$\overline{\boldsymbol{\mathcal{V}}} = \frac{1}{2}(\boldsymbol{\mathcal{V}}_1 + \boldsymbol{\mathcal{V}}_2) \tag{19}$$

where addition and multiplication are pointwise. Let

$$\boldsymbol{T} = (2\boldsymbol{G} - \boldsymbol{I})(2\boldsymbol{F} - \boldsymbol{I}). \tag{20}$$

We are looking for a solution $\boldsymbol{\mathcal{V}}^* \in \mathbb{R}^{M\times N\times B\times 2}$ that satisfies

$$\boldsymbol{T}(\boldsymbol{\mathcal{V}}^*) = \boldsymbol{\mathcal{V}}^*. \tag{21}$$

This fixed point yields the uncompressed tensor:

$$\boldsymbol{\mathcal{X}}^* = \overline{\boldsymbol{\mathcal{V}}}^*. \tag{22}$$

Mann iterations can help to evaluate the fixed point:

$$\boldsymbol{\mathcal{V}}^{k+1} = (1-\rho)\boldsymbol{\mathcal{V}}^k + \rho\boldsymbol{T}(\boldsymbol{\mathcal{V}}^k) \tag{23}$$

for a fixed parameter $\rho \in (0, 1)$. Addition and multiplication are defined pointwise. Algorithm 5 outlines this procedure to apply consensus equilibrium for compressive matrix completion.

Algorithm 5 Consensus equilibrium for compressive matrix completion

1: Initialize $\boldsymbol{\mathcal{V}}^0 \in \mathbb{R}^{M\times N\times B\times 2}$ to any value.
2: $k \leftarrow 0$
3: **while** not converged **do**
4: $\quad \boldsymbol{\mathcal{V}}^{k+1} \leftarrow (1-\rho)\boldsymbol{\mathcal{V}}^k + \rho\boldsymbol{T}(\boldsymbol{\mathcal{V}}^k)$
5: $\quad k \leftarrow k+1$
6: **end while**
7: $\boldsymbol{\mathcal{X}} \leftarrow \overline{\boldsymbol{\mathcal{V}}}^k$

To compare two tensors $\boldsymbol{\mathcal{U}}$ and $\boldsymbol{\mathcal{V}}$ of the same size $M \times N \times B$, we define the mean squared error as

$$\text{MSE}(\boldsymbol{\mathcal{U}}, \boldsymbol{\mathcal{V}}) = \frac{1}{M\times N\times B}\sqrt{\sum_{i,j,k}^{M,N,B} (\boldsymbol{\mathcal{U}}_{i,j,k} - \boldsymbol{\mathcal{V}}_{i,j,k})^2} \tag{24}$$

where $\boldsymbol{\mathcal{U}}_{i,j,k}$ denotes the (i, j, k) entry of $\boldsymbol{\mathcal{U}}$.

3. EXPERIMENT

The Indian Pines dataset is a hyperspectral image over the Purdue University agronomy farm in West Lafayette, Indiana.[24] It consists of a 145×145 image with $B = 220$ bands, as measured by the Airborne Visible/Infrared Imaging Spectrometer (AVIRIS). The uncompressed tensor $\boldsymbol{\mathcal{X}}$ is reduced to a size of $5 \times 5 \times 220$ by uniformly downsampling the original dataset by a factor of 32 along the spatial dimensions. This smaller size enables faster computations while still illustrating the concept.

We take $R = 110$ measurements to encode $B = 220$ bands for a compression ratio of $\kappa = 50\%$. The sampling matrix $\boldsymbol{A} \in \mathbb{R}^{R \times B}$ has uniformly distributed entries:

$$\boldsymbol{A}_{ij} \sim U(0, 1). \tag{25}$$

According to compressive sensing theory, random matrices satisfy the restricted isometry property with high probability. This enables a solution to be recovered with convex optimization. Other matrices may be substituted for $\boldsymbol{A}$ depending on the measurement system.

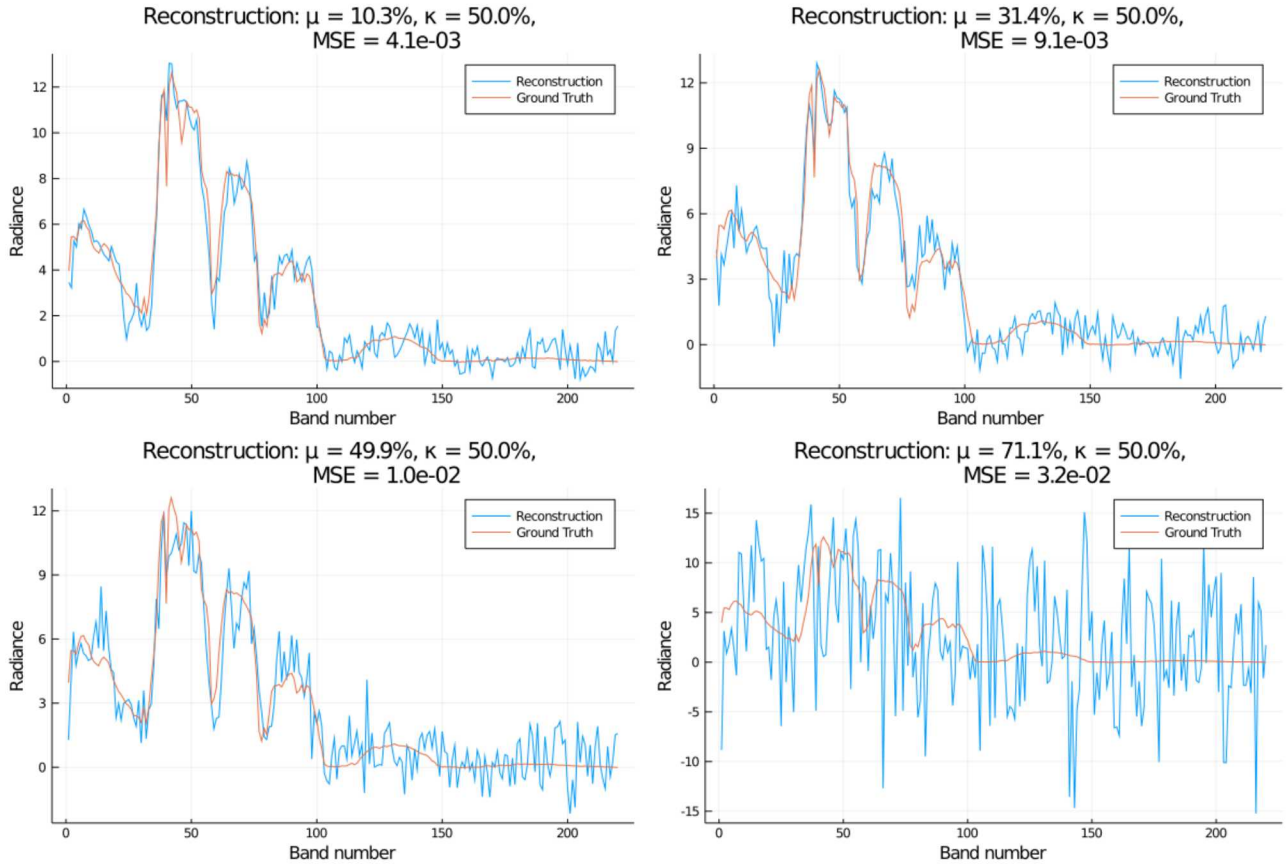

Figure 1: Reconstruction of compressive measurements with missing data. The plots show the spectra from one pixel of the Indian Pines hyperspectral data. μ denotes the fraction of missing data. In all simulations, the compression ratio $\kappa = 50\%$. Radiance is in units of [W cm^{-2} nm^{-1} sr^{-1}].

For basis pursuit, the spectra are compressed in Daubechies 8 (db8) wavelet coefficients. We set the denoising parameter $\sigma = 0.01$.

For matrix completion of the compressive measurements, we fix the rank $k = 6$. The regularization parameter $\gamma = 1 \times 10^6$, and the consensus equilibrium parameter $\rho = 0.5$. All parameters are fixed in the simulations.

The amount of missing data in the compressive measurements varies from $\mu = 10\%$ to $\mu = 90\%$ in increments of 10%. Missing entries in $\boldsymbol{\mathcal{Y}}$ are selected randomly with probability μ. In real systems, missing data may result

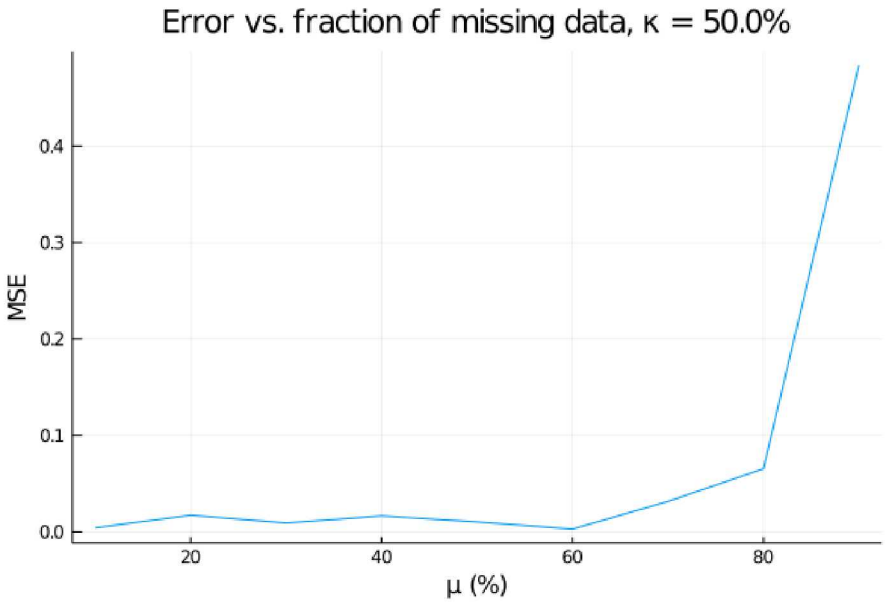

Figure 2: Error increases with the amount of missing data in the compressive space. In all simulations, the compression ratio $\kappa = 50\%$.

from transmission errors or deliberate subsampling of data. Figure 1 shows spectral reconstructions of one pixel from the Indian Pines hyperspectral data. Each plot varies the amount of missing data, including $\mu = 10\%$ through $\mu = 71\%$. The compression ratio is fixed at $\kappa = 50\%$. We use the metric for mean squared error defined in Eq. (24). This metric measures the difference between the ground truth for the uncompressed tensor and the reconstruction. Error increases with the amount of missing data in the compressive space, as plotted in Figure 2. The reconstructions show reasonable agreement with ground truth even though a majority of the data has been compressed or removed.

4. CONCLUSION

We have proposed a technique for reconstruction from incomplete compressive measurements. Our approach combines compressive sensing and matrix completion using the consensus equilibrium framework. The algorithm imposes two constraints on the solution. First, the compressed tensor should be consistent with the uncompressed tensor $\boldsymbol{\mathcal{X}}$ when it is projected onto the low-dimensional subspace. Second, the measurements should live in a low rank subspace when the missing entries are completed. These constraints allow us to solve for the uncompressed tensor when data is missing in the compressive space. We validate our approach on the Indian Pines hyperspectral dataset. The spectra are first compressed by 50%, and then tensor elements are randomly removed. The reconstructions show reasonable agreement with ground truth even though a majority of the data has been compressed or removed. This work opens up new possibilities for data reduction, compression, and reconstruction.

ACKNOWLEDGMENTS

Sandia National Laboratories is a multimission laboratory managed and operated by National Technology and Engineering Solutions of Sandia, LLC., a wholly owned subsidiary of Honeywell International, Inc., for the U.S. Department of Energy's National Nuclear Security Administration under contract DE-NA-0003525.

REFERENCES

[1] J. Romberg, "Imaging via compressive sampling," IEEE Sig. Proc. Mag., March 2008.

[2] D. J. Lee, C. F. LaCasse, and J. M. Craven, "Compressed channeled linear imaging polarimetry," Proc. SPIE 10407, 104070D (2017)

[3] D. J. Lee, C. A. Bouman, and A. M. Weiner, "Single Shot Digital Holography Using Iterative Reconstruction with Alternating Updates of Amplitude and Phase," http://www.arxiv.org/abs/1609.02978 (2016).
[4] P. Llull, et. al., "Coded aperture compressive temporal imaging," Opt. Exp. 21(9) (2013).
[5] D. J. Lee, "Compressive sensing for channeled polarimetry: Applications in spectropolarimetry and imaging polarimetry," Proc. SPIE 11130, 111300D (2019).
[6] D. J. Lee, C. F. LaCasse, and J. M. Craven, "Compressed channeled spectropolarimetry," Opt. Express 25, 32041-32063 (2017).
[7] M. Duarte, M. Davenport, D. Takhar, J. Laska, T. Sun, K. Kelly, R. Baraniuk, "Single-pixel imaging via compressive sampling," IEEE Signal Process. Mag. 25(2) (2008).
[8] E. Candes and T. Tao, "Decoding by linear programming," IEEE Trans. Inform. Theory, 51(12) 2005.
[9] C. Qiu, N. Vaswani, B. Lois, and L. Hogben, "Recursive robust PCA or recursive sparse recovery in large but structured noise," IEEE Trans. Inform. Theory 60(8) (2014).
[10] E. Candes and T. Tao, "The power of convex relaxation: Near-optimal matrix completion. IEEE Transactions on Information Theory, 56(5) (2010).
[11] C. Jin, S. Kakade, and P. Netrapalli, "Provable efficient online matrix completion via non-convex stochastic gradient descent," Advances in Neural Information Processing Systems (2016).
[12] D. J. Lee, C. F. LaCasse, and J. M. Craven, "Channeled spectropolarimetry using iterative reconstruction," Proc. SPIE 9853, 98530V (2016).
[13] S. Boyd, N. Parikh, E. Chu, B. Peleato, and J. Eckstein, "Distributed optimization and statistical learning via the alternating direction method of multipliers," Found. Trends Mach. Learn., 3 (2011).
[14] D. J. Lee and E. A. Shields, "Compressive hyperspectral imaging using total variation minimization," Proc. SPIE 10768, 1076804 (2018).
[15] A. Buades, B. Coll, and J. Morel, "A review of image denoising algorithms, with a new one," Multiscale Model. Simul. (2005).
[16] D. J. Lee, "Deep neural networks for compressive hyperspectral imaging," Proc. SPIE 11130, 1113006 (2019).
[17] D. J. Lee and A. M. Weiner, "Optical phase imaging using a synthetic aperture phase retrieval technique," Opt. Express **22**(8), 9380-9394 (2014).
[18] D. J. Lee, K. Han, H. J. Lee, and A. M. Weiner, "Synthetic aperture microscopy based on referenceless phase retrieval with an electrically tunable lens," Appl. Opt. **54**(17), 5346-5352 (2015).
[19] G. Buzzard, S. Chan, S. Sreehari, and C. Bouman, "Plug-and-play unplugged: Optimization-free reconstruction using consensus equilibrium," SIAM J. Imaging Sciences 11(6) 2018.
[20] S. Sreehari, S. Venkatakrishnan, B. Wohlberg, G. Buzzard, L. Drummy, J. Simmons, and C. Bouman, "Plug-and-play priors for bright field electron tomography and sparse interpolation," IEEE Trans. Comput. Imaging 2 (2016).
[21] T. Kolda and B. Bader, "Tensor decompositions and applications," SIAM Rev. 51(3) (2009).
[22] E. van den Berg and M. P. Friedlander, "Probing the Pareto frontier for basis pursuit solutions," SIAM J. Scientific Computing 31(2) (2008).
[23] D. Bertsimas and M. Li, "Fast Exact Matrix Completion: A Unifying Optimization Framework," J. Mach. Learning Research 2 (2019).
[24] M. Baumgardner, L. Biehl, D. Landgrebe. 220 Band AVIRIS Hyperspectral Image Data Set: June 12, 1992 Indian Pine Test Site 3. Purdue University Research Repository. doi:10.4231/R7RX991C (2015).